

# Effect of magnetic field on the burning of a neutron star

Ritam Mallick\* and Amit Singh

*Indian Institute of Science Education and Research Bhopal, Bhopal, India*

(Dated: June 14, 2019)

## Abstract

In this article, we present the effect of a strong magnetic field in the burning of a neutron star (NS). We have used relativistic magneto-hydrostatic (MHS) conservation equations for studying the PT from nuclear matter (NM) to quark matter (QM). We found that the shock-induced phase transition (PT) is likely if the density of the star core is more than three times nuclear saturation ( $\rho_s$ ) density. We have also obtained that the conversion process from NS to quark star (QS) is an exothermic process beyond such densities. The burning process at the star center most likely starts as a deflagration process. However, there can be a small density window at lower densities where the process can be a detonation one. However, at such low densities, the NM energy and QM energy are almost equal, and it is unlikely that the PT process would be an exothermic one. At small enough infalling matter velocities the resultant magnetic field of the QS is lower than that of the NS. However, for a higher value of infalling matter velocities, the magnetic field of QM becomes larger. Therefore, depending on the initial density fluctuation and on whether the PT is a violent one or not the QS could be more magnetic or less magnetic. This can have substantial observational significance because a strong magnetar can suddenly become less magnetic and would not show common magnetar properties vice-versa. The PT also have a considerable effect on the magnetic tilt of the star. For smaller velocities and densities the magnetic angle are not affected much but for higher infalling velocities tilt of the magnetic change suddenly. Such angular change can have a massive effect on the observation of the magnetars where new observation can be recorded after PT.

PACS numbers: 47.40.Nm, 52.35.Tc, 26.60.Kp, 97.10.Cv

Keywords: dense matter, equation of state, stars : magnetic field, stars: neutron, shock waves

---

\* mallick@iiserb.ac.in

## I. INTRODUCTION

One of the most challenging aspects of astrophysics is the study and understanding of compact objects. Compact objects usually refer to the family of white dwarfs, compact stars and black hole, which are formed after the gravitational collapse of a dead star. Among the compact objects compact stars (otherwise commonly known as neutron stars (NS) or quark stars (QS)) has a special significance in astrophysics because in addition to the importance of the objects themselves they also serve as a tool to improve the understanding of nuclear matter (NM) and possibly quark matter (QM) at enormous densities and low temperatures (see, e.g., [1, 2]). Thus the compact star serves as an ideal complementary approach to the study of high-temperature relativistic heavy-ion collisions.

Our understanding of compact stars has changed in the last fifty years, beginning with the discovery of pulsars [3] and connecting them with NS [4]. It was quite well understood that pulsars are nothing but spinning compact stars (CS) emitting mostly x-rays and radio waves. The central density of CS is inferred to be as high as  $3 - 10$  times nuclear saturation density. Over time different equation of state (EoS) of matter at such high density has been proposed and is being continuously refined. One of the most exciting aspects which arose from such high-density stars is the occurrence of QM in their cores where confinement to deconfinement transition takes place, resulting in QS. Therefore, CS can be of two types

- a) NS composed entirely of NM
- b) QS which have some quantity of deconfined QM in them.

While the nuclear and quark model has improved over the years, significant advancement came from the astrophysical observation.

The change has been more rapid in the last decade when the discovery and timing observation of pulsars has gained acceleration due to the advent of new generation of space-based X-ray and gamma-ray satellites (Einstein/EXOSAT). Important observation also came from the ROSAT observatory. However, a new era of thermal radiation observation started after the launching of CHANDRA and XMM-Newton Observatory. With improved telescopes and interferometric techniques, the number of observed binary pulsars is continuously increasing. Till date, we know precise masses of about 35 pulsars spanning the range from  $1.15M_{\odot}$  to  $2.01M_{\odot}$ . The radius measurement is not as precise as the masses. However, it is widely accepted that they must lie in the range between  $9 - 13$  km. The knowledge of

heaviest NS, PSR J1614-2230 and PSR J0348+0432 [5, 6] and connecting them with the existing radius bound already places a significant constraint on the EoS of matter at these extreme densities.

The possible existence of both NS and QS has been proposed long back [7–9]. The conversion of an NS to a QS is likely through a deconfined phase transition (PT). The PT can occur either soon after the formation of the NS in a supernovae explosion or during the later time through a first order PT. The phase transformation is usually assumed to begin at the center of a star when the density increases beyond the critical density. Several processes can trigger PT: slowing down of the rotating star [10], accretion of matter on the stellar surface [11] or simply cooling. Such a PT is characterized by a significant energy release in the form of latent heat, which will be accompanied by a neutrino burst, thereby cooling the star. Corresponding star transformations should lead to interesting observable signatures like  $\gamma$ -ray bursts [12–15], changes in the cooling rate [16], and the gravitational wave (GW) emission [17].

The dynamical study of PT is somewhat uncertain and even controversial [18]. In the literature one can find two very different scenarios: (i) the PT is a slow deflagration process and never a detonation [19] and (ii) the PT from confined to deconfined matter is a fast detonation-like process, which lasts about 1 ms [20]. If the process is quick burning and very violent (detonation), there could be robust GW signals coming from them which could be detected at least in the second or third generation of VIRGO and LIGO GW detectors [17, 21]. The earliest calculation [22] assumed the conversion to proceed via a slow combustion, where the conversion process depends strongly on the temperature of the star. Later, Horvath & Benvenuto [23] showed the stability of the conversion process, and found that under the influence of gravity the conversion process becomes unstable and the slow combustion can become a fast detonation. A relativistic calculation was done [24] to determine the nature of the conversion process, employing the energy-momentum conservation and baryon number conservation (also known as the Rankine-Hugoniot condition). A recent calculation of the burning process for violent shocks has also been studied [25]. However, there is still no consensus about the nature of the conversion process.

Another unique feature of compact stars is the presence of ultra-strong magnetic field at their surface. The surface field strength for almost all pulsars are of the order of  $10^8 - 10^{12}$  G. However, recent observations of several new pulsars, namely some anomalous X-ray pulsars

(AXP) and soft-gamma repeaters (SGR), have been identified to have much stronger surface magnetic fields [26, 27]. Such pulsars with strong magnetic fields are separately termed as magnetars [28, 29]. Such field is usually estimated from the observation of the NS period and the period derivative. It has also been attributed that the observed giant flares, SGR 0526-66, SGR 1900+14 and SGR 1806-20 (Palmer et al. 2005), are the manifestation of such strong surface magnetic in those stars. While magnetic fields as high as  $10^{15}$  G have been inferred at the surface of magnetars [28, 30, 31], there is indirect evidence for fields as high as  $10^{16}$  G inside the star [32].

The origin of such high magnetic field is still unknown. The magnetic field of regular old pulsars is attributed to the conservation of the magnetic flux during the core collapse of supernovae. However, they are unable to explain the strong surface fields of magnetars. The idea by Thompson and Duncan [28], suggest a dynamo process by combining convection and differential rotation in hot proto-neutron stars can build up a field of strength of  $10^{15}$  G. Recently it was proposed that magneto-rotational instability and MRI drove dynamo in hot proto-neutron stars can amplify average magnetic field strength to very high values in quite short time [33–37]. Whatever may be the origin of such magnetic fields it is clear that they would have significant impact on the physical aspect of such stars.

The aim of this present work is to study the effect of such strong magnetic field in the conversion of NS to QS. Instead of using the relativistic conservation condition we would employ magneto hydrostatic conservation condition in the HT frame [38]. We will treat the matter as an ideal fluid with an infinite conductivity. We would mostly concern ourselves with the space-like shocks, where the shock propagates with a velocity less than the speed of light. However, in some situations, there may be a fast PT (first order) where the normal vector to the surface of the discontinuity can be time-like [39]. Although it is difficult to realize time-like shocks in the astrophysical scenario, we would be interested in its theoretical implication if any.

In our investigation, we would assume that a PT takes place inside a cold NS. We assume that the formation of the new phase takes place at the center of the star due to a sudden fluctuation of the star density. The star then burns from the core to the periphery. The conversion process would be determined by the conservation equations and the EoS of the matter on either side of the front.

The paper is organized as followed. In section 2 we discuss the effect of magnetic field on

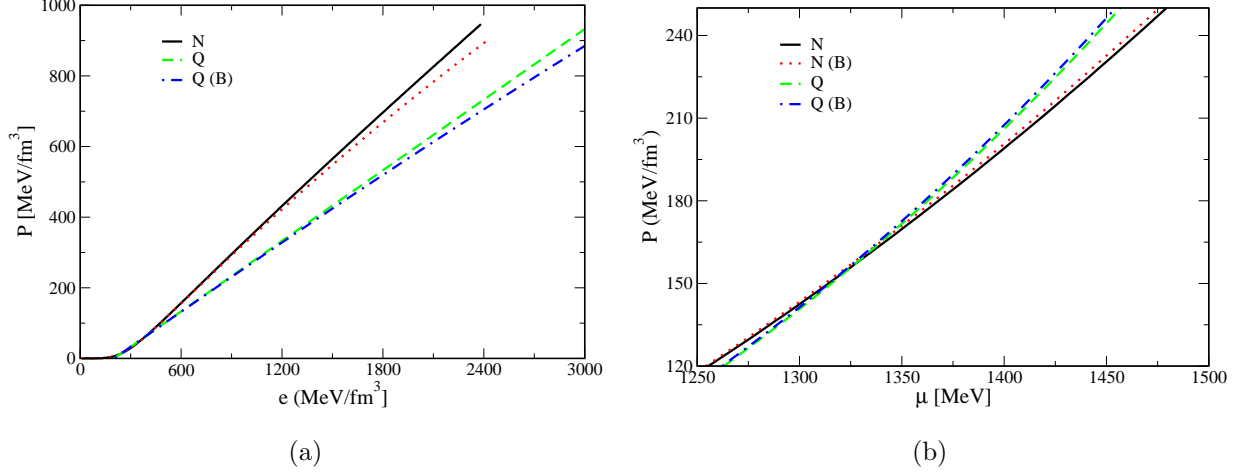


FIG. 1. (Color online) a) EoS for NM and QM are shown. N stands for NM and Q for QM. For comparison curve with magnetic field induced EoS are also shown with B. b) Pressures of NM and QM as functions of baryon chemical potential. The intersection point corresponds to the equilibrium PT from NM to QM. Similar curve with magnetic field induced EoS are also plotted following similar prescription as in plot 1a.

the EoS of a star before and after the PT keeping in mind the recent observational bound. The original star is of hadronic matter whereas the final burned state is of deconfined QM. In section 3 we discuss the effect of magnetic field on the star structure. Next, in section 4 we present the MHS conservation equation for the space-like and time-like conversion. In section 5 we show our results aiming to clarify and classify the conversion process. Finally, in section 6 we summarize our findings and discuss their potential astrophysical implications.

## II. MAGNETIC FIELD INDUCED EOSS

The PT is brought about by a sudden density fluctuation at the star core. This initiates a finite density and pressure fluctuation which propagates outwards. This fluctuation is assumed to propagate along a single very thin layer, known as PT front, converting NM to QM. Therefore, to describe the properties of NM and QM, we need EoSs. We employ such EoS which satisfies the current bound on the recent pulsar mass measurement. We use zero temperature EoS as we assume that the PT takes place due to density fluctuation in any ordinary cold pulsars. However, the final burnt QM can have finite temperature depending on the EoS of matter on either side of the PT front. For the hadronic phase we adopt

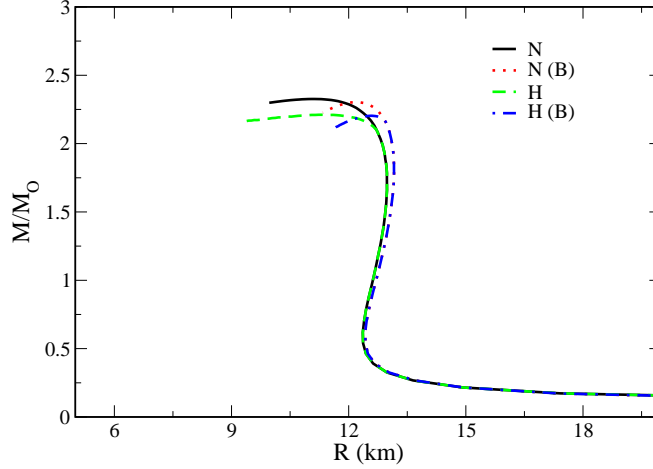


FIG. 2. (Color online) The mass-radius sequence of different compact stars (NS and HS) obtained by solving the TOV equations (N stands for NS and H for HS). Also shown in the graphs are the mass-radius sequence of magnetized stars with B.

a relativistic mean field approach which is generally used to describe the NM in CS. The corresponding Lagrangian is given in the following form [40–42] ( $\hbar = c = 1$ )

$$\begin{aligned} \mathcal{L}_H = & \sum_n \bar{\psi}_n [\gamma_\mu (i\partial^\mu - g_{\omega n}\omega^\mu - \frac{1}{2}g_{\rho n}\vec{\tau}\cdot\vec{\rho}^\mu) - (m_n - g_{\sigma n}\sigma)] \psi_n \\ & + \frac{1}{2}(\partial_\mu\sigma\partial^\mu\sigma - m_\sigma^2\sigma^2) - \frac{1}{3}b\sigma^3 - \frac{1}{4}c\sigma^4 - \frac{1}{4}\omega_{\mu\nu}\omega^{\mu\nu} + \\ & \frac{1}{2}m_\omega^2\omega_\mu\omega^\mu - \frac{1}{4}\vec{\rho}_{\mu\nu}\cdot\vec{\rho}^{\mu\nu} + \frac{1}{2}m_\rho^2\vec{\rho}_\mu\cdot\vec{\rho}^\mu + \sum_l \bar{\psi}_l [i\gamma_\mu\partial^\mu - m_l]\psi_l. \end{aligned} \quad (1)$$

The EoS contains only nucleons ( $n$ ) and leptons ( $l = e^\pm, \mu^\pm$ ). The leptons are assumed to be non-interacting, but the nucleons interact with the scalar  $\sigma$  mesons, the isoscalar-vector  $\omega_\mu$  mesons and the isovector-vector  $\rho_\mu$  mesons. The fundamental properties of NM and that of finite nuclei are used to fit the adjustable parameter of the model. In our present calculation, we use PLZ parameter set [43, 44], which usually generates massive NSs, with 12.9 km radius for  $1.4M_\odot$  star, which are in agreement with recent constraints of mass and radius [45, 46].

To describe the QM, we use simple MIT bag model [47]. The inclusion of the quark interaction in this basic model makes it possible to satisfy the present mass bound. The grand potential of the model is given by

$$\Omega_Q = \sum_i \Omega_i + \frac{\mu^4}{108\pi^2}(1 - a_4) + B \quad (2)$$

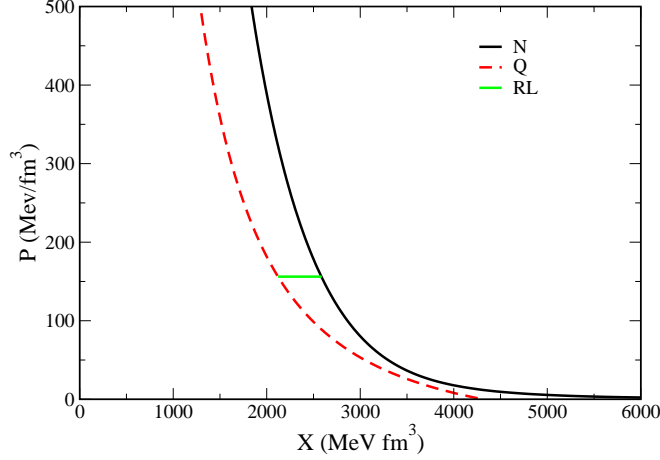


FIG. 3. (Color online) The Poisson's adiabats plotted in the  $X - P$  plane both for NM and QM (Q for QM). straight green line (RL) indicate baryon density and energy density jumps for the equilibrium PT. The graphs are shown for magnetic field induced EoS.

where  $i$  stands for quarks and leptons,  $\Omega_i$  signifies the potential for species  $i$  and  $B$  is the bag constant. The second term is for the interaction of quarks.  $\mu$  is the baryon chemical potential and  $a_4$  is the quark interaction parameter, varied between 1 (no interaction) and 0 (full interaction). We have only two quark species the  $u, d$  and quarks. The masses of the  $u$  and  $d$  quarks are 5 and 10 MeV respectively. We choose the values of  $B^{1/4} = 140$  MeV and  $a_4 = 0.55$ . We choose such parameter setting because we wanted to have PT happening beyond the saturation density. The PT from nuclear matter to quark matter is usually a two-step process. In the first step, the NM is converted to 2- flavor quark matter following the hydrodynamic conservation condition. In the next step, the 2- flavor matter is converted to 3- flavor stable quark matter via weak interaction, which is a slow process. As we are dealing with only the first process here, our matter is two flavor matter. All our results are obtained employing 2- flavor matter properties.

For magnetars, the magnetic field is also very high, and it is likely to affect the EoS of the stars. The detail of the calculation is similar to that of Mallick & Sinha [48], and for brevity, we only give the overall details here. For a magnetic field in the  $z$ -direction, the motion of the charged particles are Landau quantized in the  $x - y$  plane, and therefore the energy in the  $n$ th Landau level is given by

$$E_n = \sqrt{p_z^2 + m^2 + 2ne|Q|\mathcal{B}}. \quad (3)$$

The magnetic field similarly modifies the quark matter. The details are given in ref. [48] and we do not repeat them here. In our calculation we use a simple phenomenological density dependent magnetic field profile given by [49–51], and is parametrized as

$$B(n_b) = B_s + B_0 \left\{ 1 - e^{-\alpha \left( \frac{n_b}{n_0} \right)^\gamma} \right\}. \quad (4)$$

where,  $B_s$  is the surface magnetic field and  $B_0$  is field at infinitely high density. The surface field is assumed to be  $10^{15}$  G and central field is  $3 \times 10^{18}$ . We assume  $\alpha = 0.01$  and  $\gamma = 2$ , which is quite a gentle variation of the magnetic field inside the star. For such a variation the magnetic field at the center of the NS is about  $1.7 \times 10^{18}$  G or in Lorentz-Heaviside unit it is about  $1.2 \times 10^5$  MeV<sup>2</sup>.

The EoS of the NM and QM are plotted in fig 1a. In the same figure, we also plot the magnetic field induced EoS. We find that both the NM and QM EoS gets softer due to the magnetic field. The equilibrium PT point between the two phases can be calculated by plotting the pressure of the two phases as a function of chemical potential. The point of crossing of the two curves gives the PT point. Below the crossing point, the matter is hadronic and above it is quark (as shown in fig 1b). We find that even for magnetic induced NM and QM EoS the crossing point does not change much. The PT is implemented assuming Maxwell’s construction. The TOV equations are solved to obtain the star sequence of the hybrid stars (fig 2). The low mass stars are all pure hadronic, and the two curve overlap as the central density in these stars is not high enough to have PT. However, once the central density crosses the threshold value, QM stars to appear in their core and we obtain a separate branch, as the mass and radius both differ from the NSs. It is easy to observe that the PLZ model generates quite massive stars, the maximum being  $2.4 M_\odot$  with a radius about 11.5 km. The hybrid stars are less massive than the pure NS as they have quark matter inside then.

The EoS and the equilibrium PT can also be represented in the form of Poisson adiabats as shown in fig 3. The pressure is plotted as function of parameter  $X$  given by  $X \equiv (\epsilon + p)/n_b^2$ . The straight horizontal line connecting the two phases represents equilibrium PT. As we go towards the star core the pressure increases whereas the value of  $X$  decreases. The  $X$  value of NM is larger than that of QM because of the same value of pressure the density of QM is higher. In fig. 3, there is only equilibrium PT, and as QM EoS is less stiff than the NM EoS, the taub adiabat curve lies on the left of nuclear adiabat. The RL is also horizontal meaning



equilibrium PT, where there is density jump but no pressure jump. If we somehow choose the QM EoS to be more stiff in the high density regime by varying the bag constant and/or the coupling  $a_4$  term then we could have QM Taub adiabat on the right of the NM curve as obtained by Furusawa et al. [52, 53]. However, for normal cases it is highly unlikely.

During the PT there is a jump in the value of  $X$ , which becomes stronger at large densities. The equilibrium PT is difficult in old cold pulsars unless there is some sudden fluctuation in the thermodynamic quantities which can grow to give a step-like feature. We assume such step-like discontinuity generated near the star center and which propagates outwards bringing about a PT. The PT front burns the NM and leaves behind a compressed quark core. At relatively low-density region the discontinuity diminishes, and PT fronts stop. It is also assumed that the discontinuity happens only in a very thin layer in comparison to the star radius.

### III. MAGNETIC FIELD ON THE STAR STRUCTURE

In the present work, our main aim is to study the effect of strong magnetic fields in the PT of compact stars. Such strong magnetic field would also invoke significant mass modification and structural change in compact stars. The details of the calculation can be found in our previous paper [49]. Here we only mention the basic details and study their effect on the given stars sequences. The deformation of the star mainly arises due to non-uniform magnetic pressure. In the rest frame of the fluid, the magnetic field is in the z-direction, the energy density and pressure are given by

$$\varepsilon = \varepsilon_m + \frac{B^2}{8\pi} \quad (5)$$

$$P_{\perp} = P_m + \frac{B^2}{8\pi} \quad (6)$$

$$P_{\parallel} = P_m - \frac{B^2}{8\pi}. \quad (7)$$

where,  $\varepsilon$  is the total energy density,  $\varepsilon_m$  is the matter-energy density and  $\frac{B^2}{8\pi}$  is the magnetic stress.  $P_{\perp}$  and  $P_{\parallel}$  are the perpendicular and parallel components of the total pressure concerning the magnetic field.  $P_m$  is the matter pressure.

The total pressure in both the direction can be written in a single equation in terms of spherical harmonics

$$P = P_m + [p_0 + p_2 P_2(\cos\theta)]. \quad (8)$$

$p_0 = \frac{B^2}{3.8\pi}$  is the monopole contribution and  $p_2 = -\frac{4B^2}{3.8\pi}$  the quadrupole contribution of the magnetic pressure.

Similarly the metric describing a axially symmetric star can be formulated as a multipole expansion

$$ds^2 = -e^{\nu(r)}[1 + 2(h_0(r) + h_2(r)P_2(\cos\theta))]dt^2 \quad (9)$$

$$+e^{\lambda(r)}[1 + \frac{e^{\lambda(r)}}{r}(m_0(r) + m_2(r)P_2(\cos\theta))]dr^2 \quad (10)$$

$$+r^2[1 + 2k_2(r)P_2(\cos\theta)](d\theta^2 + \sin^2\theta d\phi^2), \quad (11)$$

where  $h_0, h_2, m_0, m_2, k_2$  are the corrections up to second order.

The Einstein field equations can be solved to find the metric potentials in terms of perturbed pressure and hence can be solved to calculate the mass modification and axial deformation. To solve the Einstein equation we use those as mentioned above density-dependent magnetic field profile of the star.

Using the given prescription, we calculate the stars sequence for NS and HS. In fig 2 we find that such strong magnetic fields significantly changes the mass-radius nature. The effect of magnetic field on the EoS makes it softer which would eventually reduce the maximum mass of the star. However, the magnetic force on the TOV equation tends to increase the mass of the star. Ultimately, by the action of this two effect the maximum mass of the star does not change much, however, it has a considerable impact on the star radius.

#### IV. FLUID DYNAMIC CONSERVATION CONDITIONS

The differential form of energy-momentum conservation law for a fluid dynamical system is given by

$$D_\mu T^{\mu\nu} = 0 \quad (12)$$

where,

$$T^{\mu\nu} = wu^\mu u^\nu - pg^{\mu\nu}. \quad (13)$$

$w$  is the enthalpy ( $w = \epsilon + p$ ),  $u^\mu = (\gamma, \gamma v)$  is the normalized 4-velocity of the fluid and  $\gamma$  is the Lorentz factor.  $g^{\mu\nu}$  is the metric tensor chosen as  $(1, -1, -1, -1)$  using standard flat space-time convention. Along with this the baryon number is also conserved for an isolated system such as CSs. The conservation laws can also be realized in the form of discontinuous

hydrodynamical flow usually in shock waves. We assume that the PT happens as the single discontinuity fronts propagate separating the two phases. Therefore we denote “ $h$ ” as the initial state ahead of the shock (NM) front and “ $q$ ” as the final state behind the shock (QM).

Across the front, the two phases are related via the energy-momentum and baryon number conservation. The relativistic conservation conditions for the space-like (SL) and time-like (TL) shocks are derived from the above-generalized equations [38, 39, 54].

a. Space-like

$$w_h \gamma_h^2 v_h = w_q \gamma_q^2 v_q, \quad (14)$$

$$w_h \gamma_h^2 v_h^2 + p_h = w_q \gamma_q^2 v_q^2 + p_q, \quad (15)$$

$$n_h v_h \gamma_h = n_q v_q \gamma_q \quad (16)$$

b. Time-like

$$w_h \gamma_h^2 - p_h = w_q \gamma_q^2 - p_q, \quad (17)$$

$$w_h \gamma_h^2 v_h = w_q \gamma_q^2 v_q, \quad (18)$$

$$n_h \gamma_h = n_q \gamma_q \quad (19)$$

However, when strong magnetic fields are present, the conservation condition gets modified. It now has both matter and magnetic contributions [38]. Infinitely conducting fluid assumption makes the electric field to disappear. Also, the conservation is solved in a particular frame called HT frame (HT) [55] where the fluid flows along the magnetic lines, and there are no  $\vec{u} \times \vec{B}$  electric fields. In this framework, the magnetic field and the matter velocities are aligned. We assume that  $x$ -direction is normal to the shock plane. The magnetic field is constant and lies in the  $x - y$  plane. Therefore the velocities and the magnetic fields are given by  $v_x$  and  $v_y$  and by  $B_x$  and  $B_y$  respectively. The angle between the magnetic field and the shock normal in the HT frame is denoted by  $\theta$ .

Therefore the conservation conditions now reads as

a. Space-like

$$w_h \gamma_h^2 v_{hx} = w_q \gamma_q^2 v_{qx}, \quad (20)$$

$$w_h \gamma_h^2 v_{hx}^2 + p_h + \frac{B_{hy}^2}{8\pi} = w_q \gamma_q^2 v_{qx}^2 + p_q + \frac{B_{qy}^2}{8\pi}, \quad (21)$$

$$w_h \gamma_h^2 v_{hx} v_{hy} - \frac{B_{hx} B_{hy}}{4\pi} = w_q \gamma_q^2 v_{qx} v_{qy} - \frac{B_{qx} B_{qy}}{4\pi}, \quad (22)$$

$$n_h v_{hx} \gamma_h = n_q v_{qx} \gamma_q. \quad (23)$$

b. Time-like

$$w_h \gamma_h^2 - p_h + \frac{B_{hy}^2}{8\pi} = w_q \gamma_q^2 - p_q + \frac{B_{qy}^2}{8\pi}, \quad (24)$$

$$w_h \gamma_h^2 v_{hx} = w_q \gamma_q^2 v_{qx}, \quad (25)$$

$$w_h \gamma_h^2 v_{hy} = w_q \gamma_q^2 v_{qy}, \quad (26)$$

$$n_h \gamma_h = n_q \gamma_q. \quad (27)$$

For the HT frame we also have

$$\frac{v_{hy}}{v_{hx}} = \frac{B_{hy}}{B_{hx}} \equiv \tan \theta \quad (28)$$

$$\frac{v_{qy}}{v_{qx}} = \frac{B_{qy}}{B_{qx}} \equiv \tan \theta_r. \quad (29)$$

The assumption of infinite conductivity gives the electric field to be zero. The Maxwell equation of no monopoles  $\nabla \cdot \vec{B} = 0$  gives

$$B_{hx} = B_{qx}. \quad (30)$$

The TL conservation conditions lead to some exciting results in HT frame, which can be even obtained analytically. Dividing eqn. 2 by eqn. 3, we get

$$\frac{v_{hy}}{v_{hx}} = \frac{v_{qy}}{v_{qx}}. \quad (31)$$

Combining this with eqn. 5 and eqn. 6, we have

$$\frac{B_{hy}}{B_{hx}} = \frac{B_{qy}}{B_{qx}}. \quad (32)$$

But eqn. 7 says  $B_{hx} = B_{qx}$ , therefore we have  $B_{hy} = B_{qy}$ .

Therefore eqn. 1 now becomes

$$w_h \gamma_h^2 - p_h = w_q \gamma_q^2 - p_q \quad (33)$$

Same as the non magnetic case.

Eqn. 2 and 3 can be combined in a single equation

$$w_h \gamma_h^2 v_h = w_q \gamma_q^2 v_q \quad (34)$$

Therefore, the TL conservation equation remains the same as the non magnetic case. The magnetic field does not affect the TL PT or discontinuity. In our previous work [38] we found somewhat similar result numerically, but here we can work them out even analytically. The conservation condition is such that the magnetic field does not affect TL shocks and only matter properties govern them.

## V. RESULTS

### A. SL shocks

Fluctuation of the thermodynamic quantities at the center of the star starts the PT. Let us first examine all the features of a space-like shock which is common in the astrophysical environment. Later we will discuss the TL shock. The PT would depend on the process being exothermic or endothermic. At the center of the star first there is a deconfinement transition, and then there is conversion to stable QM (3- flavor). At a certain point as the matter converts from NM to QM (2- flavor) there is a sharp change in the thermodynamic variables (like density, pressure, etc.). From here on QM would imply 2- flavor QM unless stated otherwise. The propagation of the PT front depends on the energy difference between the NM and QM. If the energy of the NM is greater than that of the QM, then the conversion is exothermic, and shock-like features can develop. However, the energy difference depends on the EoS of NM and QM, the baryon density at which the PT is taking place and also on the velocity of the shock front. The above conservation conditions are written in the rest frame of the conversion front. We solve our problem in this frame and go the global frame where QM is at rest. In our calculation, for the front rest frame, NM velocity is represented as  $v_h$  and QM velocity as  $v_q$ . In the global frame, NM velocity is given by  $v_n$  and front velocity as  $v_f$ . In this global frame the NM moves toward the center with velocity  $v_n = (v_h - v_q)/(1 - v_h v_q)$ . The front velocity near the center can assumed to be  $v_f = -v_q$ , where  $v_h$  and  $v_q$  are the quantities in the HT frame.

The equilibrium PT from NM to QM happens at around 3.3 times nuclear saturation density for our chosen set of EoS. Therefore we want to examine the shock-induced PT around this point for comparison. Therefore, we choose shock induced PT happening at 3 times and 4 times saturation density  $\rho_s$ . The magnetic field at these points can be calculated from our chosen magnetic field profile. The magnetic field  $B$  at  $3\rho_s$  is  $6 \times 10^{17}$  G ( $4.3 \times 10^4$  MeV<sup>2</sup>) and at  $4\rho_s$  is  $1 \times 10^{18}$  G ( $7 \times 10^4$  MeV<sup>2</sup>).

In this calculation, we would see the evolution of our relevant parameters regarding  $v_n$  and nuclear density  $\rho_b$ . For such analysis first we have to know how  $v_h$  and  $v_f$  varies with  $v_n$ . The velocity variation is shown in fig 4. We see that initially as  $v_n$  increases from 0 to 0.1 there is a sharp rise in  $v_h$  from 0 to 0.5 after which the slope of  $v_h$  decreases and

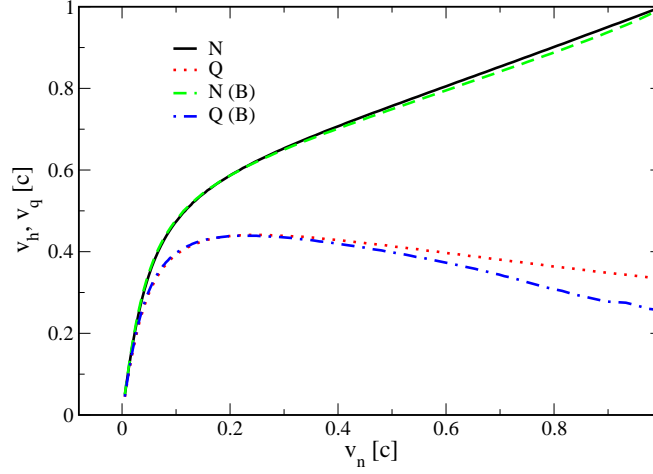


FIG. 4. (Color online) The variation of  $v_h$  and  $v_q$  as a function of  $v_n$  is shown. a) Solid (without B) and dashed (with B) curve corresponds to  $v_h$  and dotted (without B) and dash-dotted (with B) curve corresponds to  $v_q$ . Curves are shown for  $\mu = 4\mu_n$ .

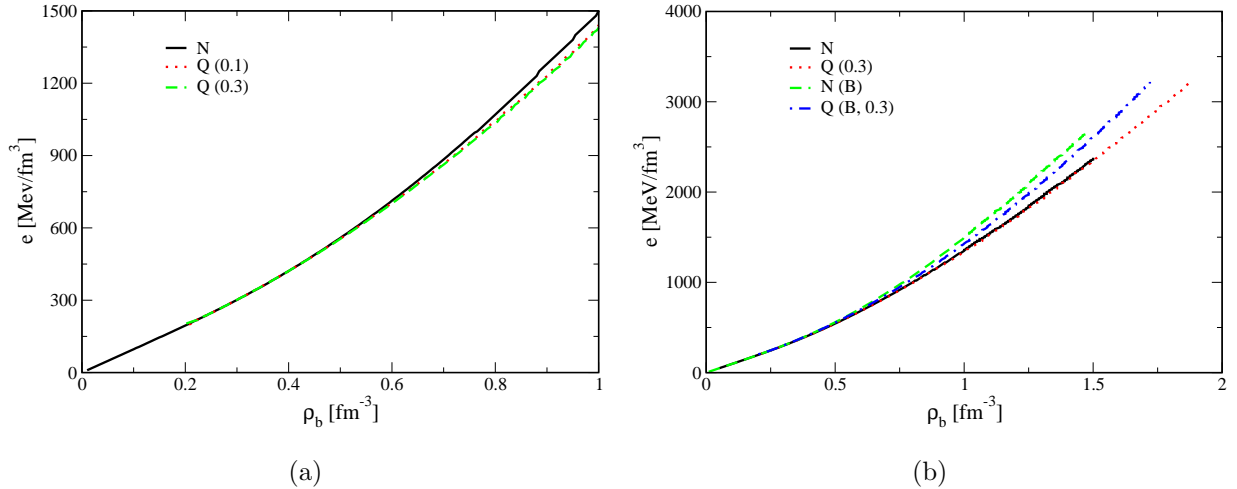


FIG. 5. (Color online) The energy density of the NP and QP as a function of baryon density are shown. a) Curves without magnetic field contribution, plotted for two given values of  $v_h$ , 0.1 and 0.3. b) Curves with contribution from magnetic field are shown with  $v_h = 0.3$ .

it gradually goes to 1 as  $v_n$  reaches 1. However, the value of  $v_h$  is always greater than  $v_n$ . The difference is high at low values of velocity and decreases as velocity increases. In other words, we can say that initially as  $v_h$  increases, the value of  $v_n$  does not change much and only after  $v_h$  goes beyond 0.5 that the value of  $v_n$  increases rapidly to match the value of  $v_h$  as they both go to 1. On the other hand, if we see the variation of  $v_f$  (which is same as  $v_q$

only the direction changes) we find that initially  $v_f$  rises rapidly to attain a maximum value of 0.44 at  $v_n = 0.2$  and from there it decreases slowly to attain value  $1/3$  as both  $v_n$  and  $v_f$  goes to 1. Near the center of the star, the velocity of the incoming matter is largest. As the shock wave propagates outwards from the center, the incoming matter velocity decreases but the front velocity increases gradually. However, after  $v_n$  becomes less than 0.2, the front velocity drops rather quickly and vanishes at  $v_n \rightarrow 0$ . It is interesting to note that the conservation conditions act in such a way that even without any dissipation mechanism there is some deceleration which drives the front velocity to zero at some point inside the star, corresponding to an equilibrium configuration with the static phase boundary. The  $v_h$  and  $v_q$  with magnetic field follows the curve closely for the nonmagnetic case, but their value at any  $v_n$  is slightly smaller than their nonmagnetic counterpart. The magnetic field slows front velocity or the speed of the conversion. Thus the PT happens slowly for magnetars than in normal NSs.

If there is a sudden fluctuation of matter at high density then the PT is no longer an equilibrium PT. Such delayed PT can occur at higher densities and can be a violent one. Such PT would depend primarily on the energy difference between hadronic state and the shocked quark state. In fig 5a we see that the energy of the NM is considerably higher than the energy of the QM (corresponding to a particular density) only beyond  $3\rho_s$ . Therefore the PT beyond this point is an exothermic one, and shock-like features can develop. We also see that the QM does not go to very low densities because as the PT occurs, the burned matter is compressed, thereby increasing its density. We also find that at densities below  $2\rho_s$  the energy difference between the un-shocked and shocked phases becomes almost equal. Beyond these densities inside the star, it is difficult for the matter to undergo PT. At such densities it is expected that the dynamical shock-front would decelerate and ultimately stop. However, such analysis can only be done once we do the full dynamic calculation, which is beyond the scope of this article. We have shown curves for two different incoming hadronic velocities ( $v_h$ ), and the behavior of the curves does not change much. In fig. 5b we show similar curves but with contribution from magnetic energy. The magnetic energy adds to the matter energies and makes the curves stiffer. However, the PT is still exothermic.

The strength of the magnetic field in the NM is input. Whereas, the magnetic field strength in the QM is obtained by solving the conservation conditions. The strength of  $B$  in QM would determine whether the resultant star would become more or less magnetic

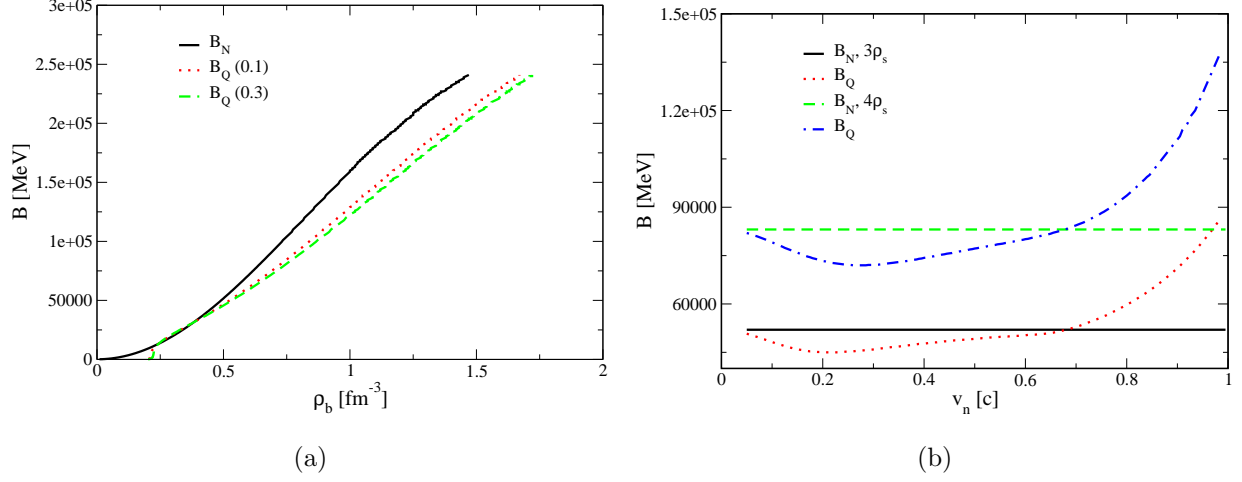


FIG. 6. (Color online) Magnetic field in the NP and QP are shown as a function of  $\rho_b$  and  $v_n$ . a) Solid line is for NP and the dotted and dashed lines are for QP with  $v_h = 0.1$  and  $v_h = 0.3$  respectively. b) Similar set of curves are plotted as a function of  $v_n$  for two different  $\rho_b$ ,  $3\rho_s$  and  $4\rho_s$ . Quantities with subscript  $N$  corresponds to NP and with subscript  $Q$  corresponds to QP.

due to the burning process. In our previous calculation [48] we have seen that QS would be less magnetic than an NS. However, in that calculation only the magnetic field contribution came from the EoS, however, in the present study we refine our calculation by solving the magnetohydrostatic conditions (conservation conditions have magnetic field exclusively) with magnetic induced EoS.

We have studied the magnetohydrostatic conservation equations when the magnetic field is at an angle  $\theta = 30^\circ$ . In usual pulsars, the magnetic axis is slightly tilted from the body axis. It has been argued by Flowers & Ruderman [56] that at the birth the tilt angle is small and with time it grows as the stars slow down. Another group [57] presented significantly different picture. However, the recent study argued [58–60] that the spin angle is either small (less than  $40^\circ$ ) or very large (greater than  $80^\circ$ ). If the magnetic field is perpendicular to the shock front, then there is no effect as then we would only have  $x$ -component of magnetic field. From Maxwell's equation, they are equal in the burnt and unburnt matter (eqn 29). The change in the total magnetic field is only due to the difference in the magnetic field in the  $y$ -direction. Therefore, for more wide tilt angle the magnetic field would not have much effect on the PT front. Thus, the compelling case to study would be when the magnetic field is less than  $40^\circ$ . For a conservative approach we have assumed the magnetic tilt to be  $30^\circ$ .



In fig 6 we plot the initial and final magnetic field as a function of both density and  $v_n$ . In fig 6a we plot the magnetic field as a function of density for two incoming matter velocities, 0.1 and 0.3. As argued from the energy diagrams we conclude that the PT would only be possible at densities beyond 3 times saturation density. At such high densities, the incoming matter velocities would not be very high, and therefore we choose  $v_n$  to be small. From fig 6a, we find that the magnetic field in the burned QM is smaller than the magnetic field in the NM. As the density increases the magnetic field in the burned matter becomes much lower. The change in magnetic field across the two sides is about 10 – 15%, at the core of the stars. This change in the magnetic field may be because the magnetic field which arrives in eqn. 21 of the conservation equations acts in the opposite direction of the matter contribution. It somehow opposes the PT. Therefore, some amount of magnetic energy is also spent in continuing the PT process. Therefore, the magnetic field in the QM is smaller. As the velocity of the incoming matter increases the magnetic field in the QM decreases much further.

Next, we plot the magnetic field on two sides as a function of  $v_c$  in fig 6b for two densities. We see that initially at smaller values of  $v_c$  the magnetic field in the QM decreases further below that of NM and attains a minimum value at around  $v_n = 0.2 - 0.3$  (corresponding to  $v_h = 0.48 - 0.65$ ). From there onwards the magnetic field in QM increases and at values greater than  $v_n = 0.7$  ( $v_h = 0.85$ ) the magnetic field in the QM becomes greater than that of NM (there is a crossing in the curves). The nature of the curves remains almost the same for both sets of densities. Such behavior may be because at such  $v_n$  the value of  $v_h$  becomes quite high, and then the conservation condition is driven mostly by the matter enthalpy and pressure than that of the magnetic force. This is quite a significant results because if the shock-induced PT is not very violent ( $v_n$  is small), then the QS is less magnetic than the NS, however, if the shock-induced PT is fierce then the QS is more magnetic than the NS.

Another interesting outcome of the phase transition which is only present for MHS calculation is the angle between the magnetic field and shock front. If the star is more or less spherical, then the angle between the body axis and magnetic axis  $\theta$  will also be the angle between the magnetic field and shock front. Therefore, the incident angle or the angle  $\theta_i$  in the NM is  $30^\circ$ . The angle in the QM would be obtained by solving the conservation conditions and is depicted as reflected angle  $\theta_r$ . The reflected angle  $\theta_r$  changes both with  $\rho_b$  and  $v_n$ . The incident angle  $\theta_i$  is always fixed at  $30^\circ$  for a star with a magnetic field.

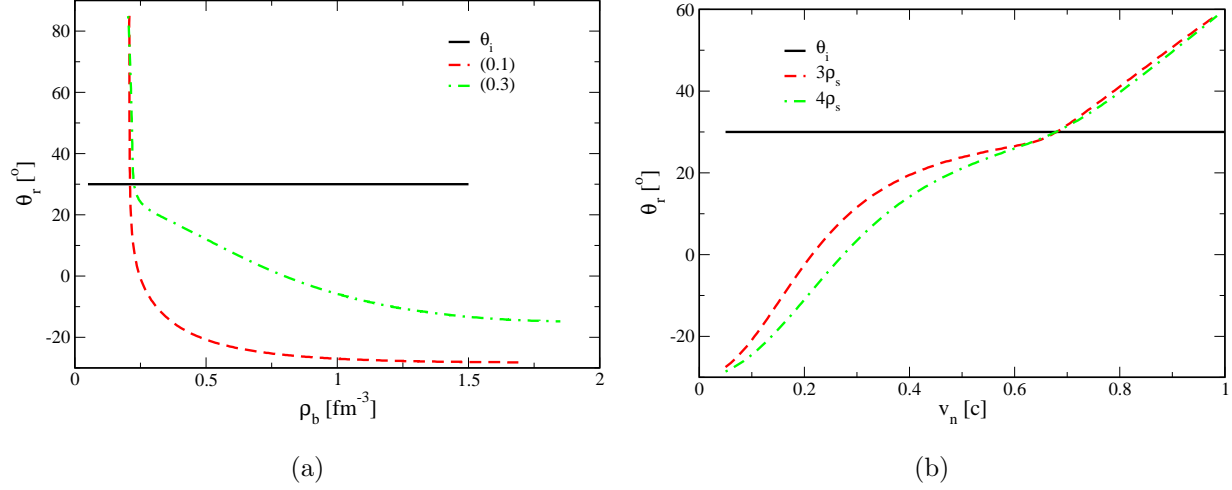


FIG. 7. (Color online) Reflected angle ( $\theta_r$ ) is plotted as a function of  $\rho_b$  and  $v_n$ . a) Solid line is for incident angle ( $\theta_i$ ) and the dashed and dash-dotted lines are for reflected angle ( $\theta_r$ ) with  $v_h = 0.1$  and  $v_h = 0.3$  respectively. b) Similar set of curves are plotted as a function of  $v_n$  for two different  $\rho_b$ ,  $3\rho_s$  and  $4\rho_s$ .

In fig 7a, we plot the reflected angle as a function of  $\rho_b$  for two incoming matter velocity  $v_h$ . At smaller densities, the reflected angle is large but falls off very fast, and at densities which are of our interest (beyond three times  $\rho_s$ ), the reflected angle is always smaller than incident angle. For small  $v_h$  the reflected angle becomes negative. The negative sign in the reflected angle means that the reflected matter velocities and magnetic field are above the plane perpendicular to the shock front (the x-axis). At very higher densities the reflected angle is always negative, and for  $v_h = 0.1$  it is negative for almost all densities of our interest. However, for  $v_h = 0.3$  and at some intermediate densities the reflected angle is positive. So there is a complete change in angular directions at higher densities. Thus, instead of pointing upwards, the matter velocities and magnetic fields point downward in the burned matter. Such features become clearer in fig 7b where we plot  $\theta_r$  as a function of  $v_n$ . We have plotted the curves for two different densities ( $3\rho_s$  and  $4\rho_s$ ). For  $3\rho_s$  we find that as the velocity increases  $\theta_r$  decreases and becomes zero at  $v_n = 0.21$  ( $v_h = 0.5$ ). After that, it increases in the positive direction and goes to about  $60^\circ$  at higher velocities. It signifies that the outflow velocity and magnetic field in the burned QM changes direction at higher speeds. The curve for  $\rho_b = 4\rho_s$  shows almost similar pattern only differing numerically. This is a fascinating result as it shows that for violent shocks where if the initial incoming matter velocity is high the resultant QS could have magnetic axis tilted in altogether another

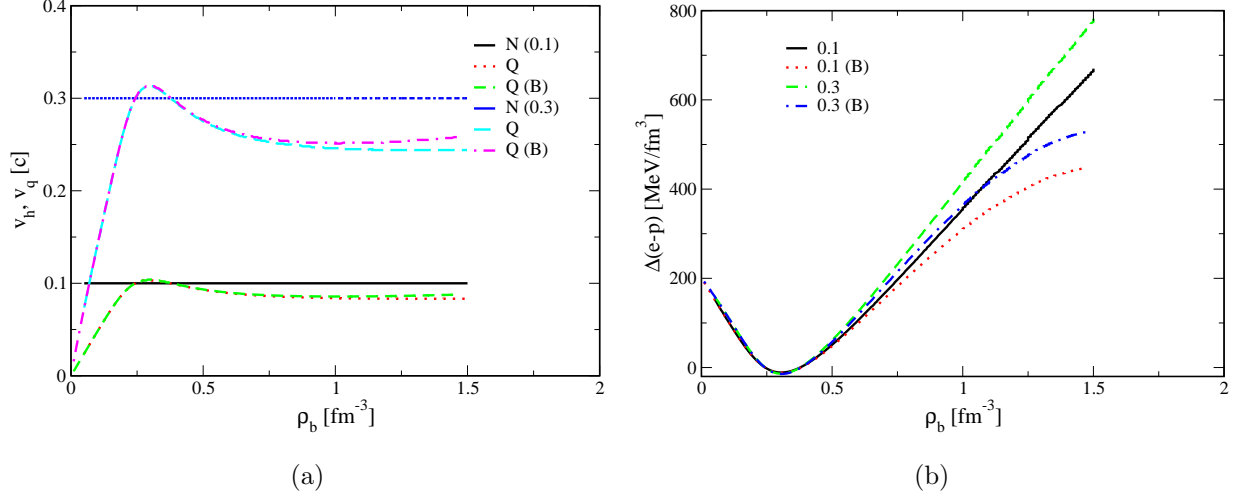


FIG. 8. (Color online) a) Curves in this figure drawn to compare  $v_h$  and  $v_q$  as a function of  $\rho_b$ . The input  $v_h$  for the magnetic and non-magnetic plots are same. Solid curve shows  $v_h = 0.1$  and the two curves below it shows the corresponding  $v_q$  with (dashed) and without (dotted) magnetic effect. The other family of three is for  $v_h = 0.3$  and its corresponding  $v_q$ 's. b) The difference of (e-p) for the QP and NP ( $\Delta(e-p)$ ) is shown as a function of  $\rho_b$ . The solid line (without magnetic effect) and the dotted line (with magnetic effect) are plotted for  $v_h = 0.1$  and the dashed and dash-dotted curves are for  $v_h = 0.3$ .

direction. Previous studies which discuss the evolution of magnetic tilt axis has calculated its development based on the spin frequency or the cooling rates which happen gradually. However, the change in the magnetic tilt brought about by PT is a sudden change and could have enormous observational significance.

The variation of matter velocities and the comparison of the burned and unburned matter velocities is a valuable tool to understand whether a shock propagation is a detonation or deflagration. If the speed of the burned matter is higher than unburnt matter, the PT is a detonation one, whereas if the velocity of the unburnt matter is higher than burned matter it is a deflagration. Detonation is very fast burning whereas deflagration is slow combustion. Another way of determining detonation and deflagration is comparing their energy and pressure. It can be classified as

- a)  $v_q > v_h$ ,  $e_q - p_q < e_h - p_h$  detonation.
- b)  $v_q < v_h$ ,  $e_q - p_q > e_h - p_h$  deflagration.

In fig 8a we plot  $v_h$  and  $v_q$  as a function of  $\rho_b$ . We have compared it for two values of  $v_h$ ,

0.1 and 0.3. We find that for the non-magnetic case at very small densities (below two times  $\rho_s$ ) the velocity of the quark matter is greater than the velocity of the nuclear matter. At such densities, the burning process can be a detonation one. However, as observed from the energy diagram at such densities, it is difficult to initiate a shock. When we draw similar plot taking into account the magnetic field the quark matter velocity is always smaller than hadronic matter velocity. Therefore, for the magnetic case the propagation is still a deflagration one. Such pattern is seen for both the incoming matter velocities. A similar conclusion is also obtained from the fig 8b. Following the condition given for determining detonation and deflagration we plot  $(e_q - p_q) - (e_h - p_h)$  (denoted as  $\Delta(e - p)$  in the fig 8b) as a function of  $\rho_b$ . The value is always positive, other than a small window at low densities where it becomes negative. The density range where a detonation process can develop is same for both the plots. The PT is always a deflagration type other than at a small window at lower densities. However, at such low densities the hadronic energy is less than the quark density as seen from fig 5. After the small window where it becomes negative the value is always positive and increases in density, meaning that the deflagration speeds up at higher densities. For  $v_h = 0.1$ , At such densities, the magnetic and non-magnetic curve almost overlap, but at higher densities, the magnetic curve lies below the non-magnetic curve. The nature of the curves remains same for all the cases.

The global nuclear matter speed and the front velocity is an important parameter for this PT. The value of  $v_n$  depends both on  $v_h$  and  $v_q$ . Although  $v_h$  is kept constant for our calculation  $v_n$  changes with  $\rho_b$  as the value of  $v_q$  changes. Therefore, it is interesting to see how the front velocity  $v_f$  and  $v_n$  changes with  $\rho_b$ . In fig 9a we have plotted the  $v_n$  and  $v_f$  as a function of  $\rho_b$  for  $v_h = 0.1$ . At low densities  $v_n$  first decreases and attains a minimum negative value at  $2\rho_s$ . Beyond this point  $v_n$  gradually increases and again becomes positive beyond  $2.5 \times \rho_s$  and then gradually attains a constant value at higher densities. The nature of  $v_f$  is completely opposite, it first increases at low densities and attains a maximum value at  $2\rho_b$  ( $v_f = 0.1 = v_h$ ) and then gradually decreases to attain almost a constant value at higher densities (which is smaller than  $v_h$ ). In the region of our interest ( $\rho_b > 3\rho_s$ )  $v_f$  is always greater than  $v_n$  and they are both smaller than  $v_h$ . The nature of both  $v_n$  and  $v_f$  are same for a magnetic star only their corresponding values are smaller than the non-magnetic star. For a magnetic star  $v_n$  never becomes negative and  $v_f$  never becomes equal to  $v_h$ . Therefore, the difference between the values of  $v_n$  and  $v_f$  when they become almost constant

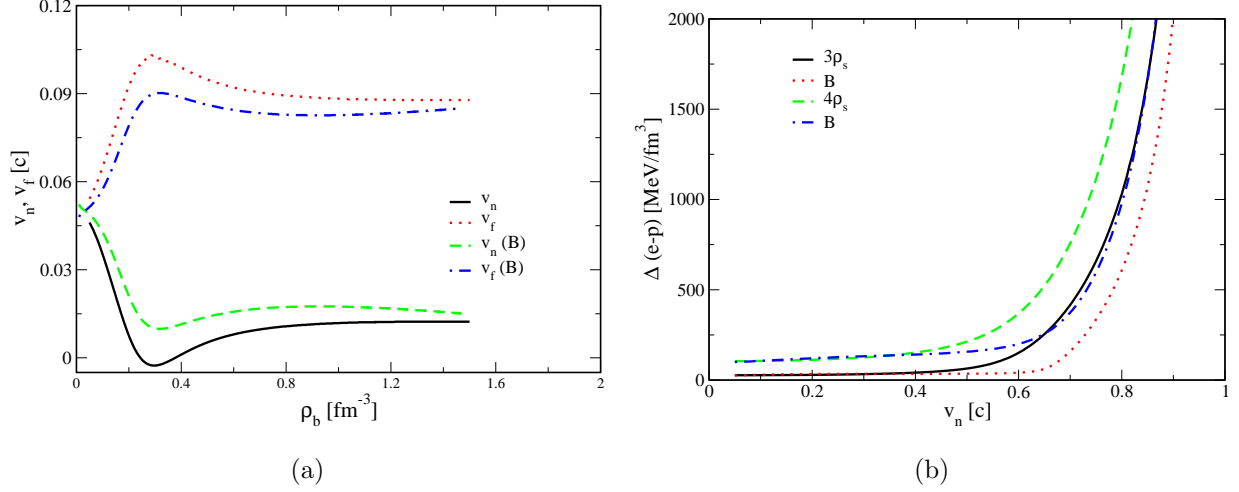


FIG. 9. (Color online) a) The incoming matter velocity  $v_n$  and the front velocity  $v_f$  in the global frame (QM rest frame) are shown as a function of  $\rho_b$ . The solid and the dashed lines are for  $v_n$  without and with magnetic effect and the dotted and dash-dotted lines are for corresponding  $v_f$ 's. Curves are plotted for  $v_h = 0.3$ . b) The difference of  $(e - p)$  for QP and NP is plotted as a function of  $v_n$ . The solid line (without magnetic effect) and the dotted line (with magnetic effect) are plotted for  $\rho_b = 3\rho_s$  and the dashed and dash-dotted curves are for  $\rho_b = 4\rho_s$ .

at high densities is smaller than the non-magnetic case.

Next in fig 9b we check the variation of  $\Delta(e - p)$  with  $v_n$  for two values of  $\rho_b$ . The value is always positive implying the burning process at such densities is always a deflagration one whatever the velocity may be. As the velocity increases the  $\Delta(e - p)$  increases, implying a strong deflagration. At very high densities the value is so large that we can infer that in any star the starting burning process is always a deflagration one. The difference is always greater for the normal NS than for magnetars implying that for magnetars deflagration is a slow one.

Nuclear to quark PT can also be realized if we plot the Taub adiabat (TA) curves. TA is a single equation which can be obtained from the conservation equations and reads as

$$(p_n + \varepsilon_q)X_q = (p_q + \varepsilon_n)X_n, \quad (35)$$

where  $X_i = w_i/n_i^2$ . The thermodynamic quantities of a given phase can be regarded as a function of this  $X$ . For a given initial state of NM (a fixed point in the curve) one can have a TA of the QM by a line in the  $X_q - p_q$  plane. The slope of the so-called ‘‘Rayleigh’’ line, connecting this initial point in the NM with the point  $(X_q, p_q)$  on the TA is related

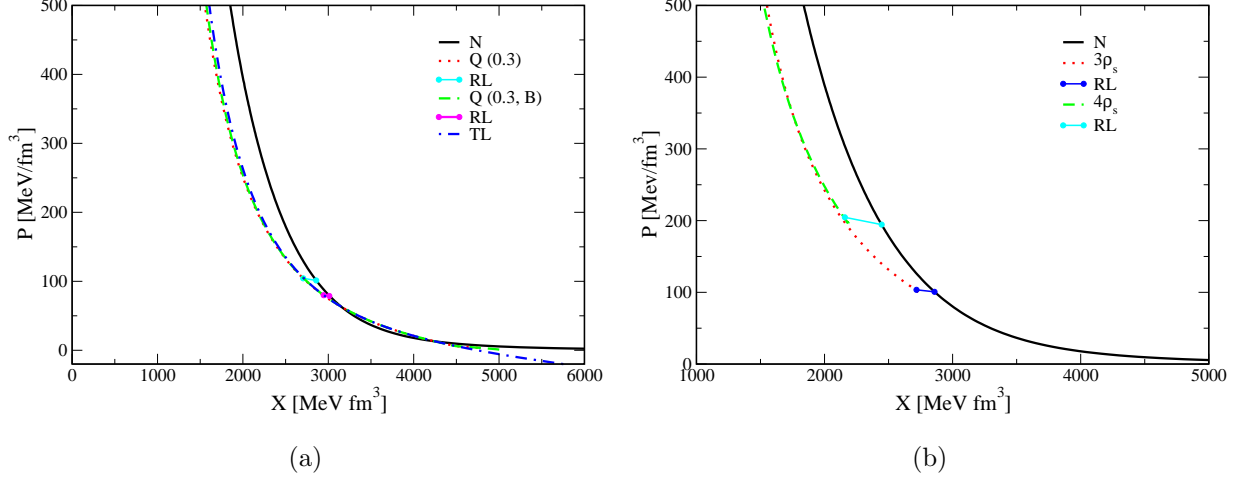


FIG. 10. (Color online) TA are shown in the  $X-P$  plane. a) Curves are plotted for a fixed  $v_h = 0.3$  and by varying the density. The horizontal lines connected with dots are the so-called RL, showing PT from NM to QM for  $\rho_b = 3\rho_s$ . TA and RL with and without magnetic field induced EoS are shown. The RL for magnetic field induced EoS happens at much lower pressure. Also shown in the graph the TA for tL shock adiabat (blue dash-dot line). b). TA obtained by varying  $v_h$  for two fixed  $\rho_b$ ,  $3\rho_s$  (dotted) and  $4\rho_s$  (dashed). The slant horizontal lines are for RL for  $v_h = 0.1$ .

to the incoming velocity  $v_h$ . As  $v_h$  increases the slope of the line increases as  $(\gamma_h v_h)^2$  [61]. Therefore, for each  $v_h$  there is a specific point on the TA corresponding to the state of compressed QP.

In fig 10a we have plotted such TA. The black line represents the initial NM EoS plotted in this plane. The shock adiabat (red dotted curve) is obtained by varying the nuclear density for a fixed incoming matter velocity ( $v_h = 0.3$ ) using the conservation conditions. Smaller density is given by higher  $X$ , and as density increases,  $X$  becomes smaller. We find that at lower densities the shock adiabat can be on the left side of the nuclear curve not observed for equilibrium PT. As the density increases, it goes to the right of the nuclear adiabat and their difference increases. The blue line represents the Rayleigh line (RL). The shock produced PT is governed by the conservation equation, and as an input, we supply the nuclear EoS (density, pressure, energy density, magnetic field and incoming matter velocity) and only the pressure-energy relation of the quark matter (effectively the EoS). Maintaining the conservation equations as an output, we obtain QM density, pressure, magnetic field and outgoing velocity. The energy is then calculated from the obtained pressure. Therefore for shock-induced PT can lie even on the left or on the right depending on the EoS. As the

hadronic matter EoS is stiffer at higher energies than QM EoS therefore usually it lies on the right of the shocked matter. However, there is a small window where it lies on the left of shock adiabat (at low energies the curve cross for both fig 1a and fig 10a)). The shock adiabat can be identified with non-horizontal RL where both density and pressure changes. In our calculation, the nuclear adiabat which we have plotted has not gone through any shock, and we only plotted its X and P values. Therefore, our calculation is in agreement with the recent papers by Furusawa et al. [52, 53].

The magnetic shock adiabat shows similar behavior, and at lower densities, it almost overlaps with the non-magnetic curve. The curve differs at higher densities. It is interesting to note that the density range where the shock adiabat lies on the left of the nuclear curve coincides with the density range where the burning becomes detonation. This is fascinating phenomena which show up in almost all the figures, however at such densities it is difficult to initiate an exothermic burning process. The RL for the magnetic adiabat lies at a lower pressure than that for non-magnetic adiabat which is expected as the magnetic EoS is softer than the non-magnetic one.

In figure 10b the shock adiabat is obtained by varying  $v_h$  for fixed values of  $\rho_b$ . The RL are shown for  $v_h = 0.3$ . Curves has been plotted for two densities  $3\rho_s$  and  $4\rho_s$ . The curve for smaller density starts from lower pressure as expected. Therefore, the RL slope is also softer than that for  $4\rho_s$ . The magnetic curve shows similar feature and has not been shown in the figure as it does not add any new physics to it.

The dynamics of the star transformation depends strongly on the ratio of densities before and after the PT, which is usually represented as  $\lambda = b_q/b_h$ . It is the ratio of quark density to hadron density. If this quantity exceeds the ratio  $3/2$ , then the matter in the vicinity of the phase boundary becomes unstable and readily converts to a new phase (QM). We plot  $\lambda$  as a function of densities in fig 11a. Other than at very low densities the value of  $\lambda$  is always less than  $3/2$  whatever the density is for both  $v_h = 0.3$  and  $v_h = 0.1$ . It signifies that the burning mechanism is always a slow deflagration and never a violent one.  $\lambda$  as a function of  $\rho_b$  for the magnetic stars also shows similar behavior.

The plot of  $\lambda$  as a function of  $v_n$  for some fixed  $3\rho_s$  and  $4\rho_s$  is shown in fig 11b. At small  $v_n$   $\lambda$  is always less than  $3/2$ .  $\lambda$  becomes greater than  $3/2$  only after  $v_n$  becomes greater than 0.6. For magnetic stars this happens even at much larger  $v_n = 0.7$ . Beyond, these values  $\lambda$  increases steadily and grows very fast. The magnetars are less prone to PT

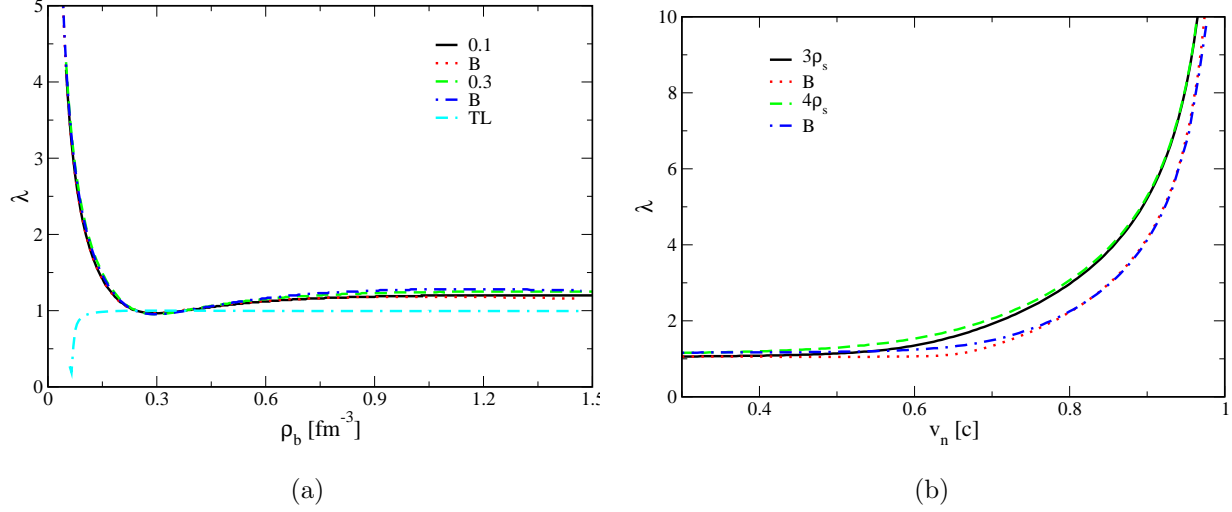


FIG. 11. (Color online) The ratio of density of QM and NM (denoted as  $\lambda$ ) at the phase boundary as a function of  $\rho_b$  and  $v_n$  are shown. a)  $\lambda$  for non-magnetic (solid and dashed line) and magnetic (dotted and dash-dotted line) are compared for two values of  $v_h$ .  $\lambda$  for TL shocks is also shown in the figure. b)  $\lambda$  for non-magnetic (solid and dashed line) and magnetic (dotted and dash-dotted line) are compared for two values of  $\rho_b$ .

than regular NS.

The primary cause of the front propagation is due to the energy and pressure discontinuity at the phase boundary. The higher the discontinuity, the more probable is the chances of shock propagation. In the rest frame of the front, if the pressure and density are higher on the left side (NM) than on the right (QM), the discontinuity would move towards the right. In the case of a star, the density and pressure of the burned QM are higher than that of unburned NM. Therefore the shock would propagate to the NM converting more and more NM to QM. In fig 12a we plot the pressure discontinuity ( $\Delta P = P_q - P_h$ ) as a function of baryon density and in fig 12b we plot it as a function of  $v_n$ . From fig 12a it is clear that the pressure discontinuity is higher at high densities and decreases as we go to the lower densities. It even becomes negative at the small density window that has been discussed earlier. For magnetic stars, the pressure difference  $\Delta P$  becomes more significant than the previous case. For higher  $v_h$   $\Delta P$  is higher which is also clear from fig 12b. We find that as  $v_c$  increases the pressure difference increases and increases it increases asymptotically at velocities beyond to 0.8. Therefore, if the velocity of the incoming matter is very high shock induced PT is much easier to form and small fluctuation gives rise to stiff shocks.



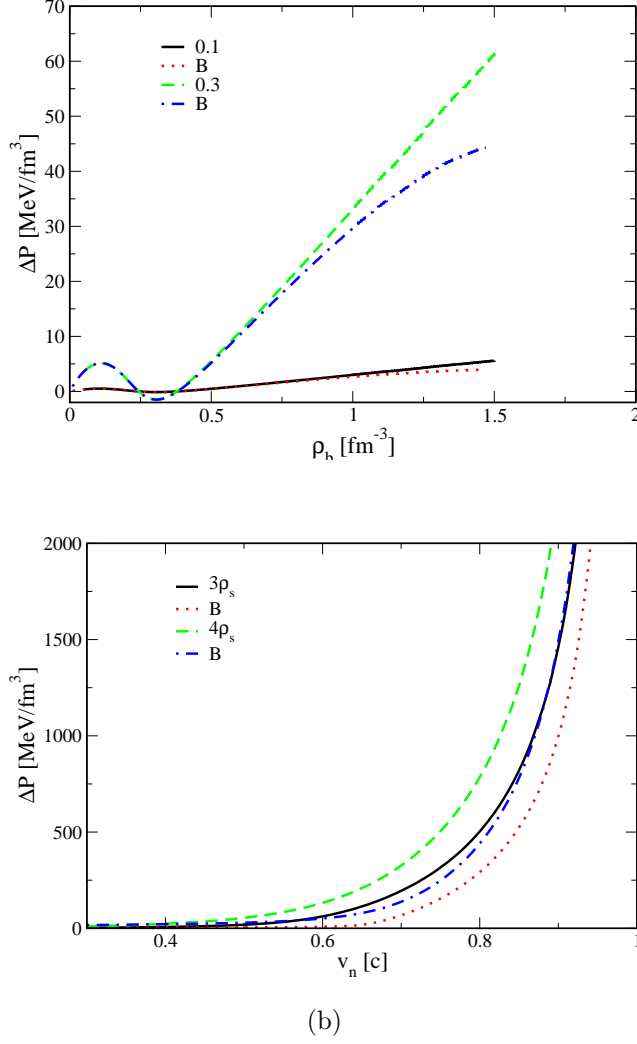


FIG. 12. (Color online) Difference between the pressure in the QP and NP ( $\Delta P$ ) as a function of  $\rho_b$  and  $v_n$  are drawn. Curve with and without magnetic field effect are shown with nomenclature same as the previous figure. a) Curves are plotted for two different  $v_h$ , 0.1 and 0.3. b) Curves are plotted for two  $\rho_b$ ,  $3\rho_s$  and  $4\rho_s$ .

## B. TL shocks

Section IV shows that the magnetic field does not affect TL shock if we assume infinite conductivity. All the conservation condition remains the same. Let us see here how the TL shock compares with the SL shock in the astrophysical scenario. The TL shock also satisfies the TA, and comparing it with SL shocks we find no such significant difference, only that it goes to much lower pressure values (fig 10a). Fig 13a shows that  $\lambda$  for TL PT is close to one for all densities, therefore, it is challenging to start TL shock at star center. It is true

that for TL shocks the discontinuity in the thermodynamic quantities does not proceed as a step-like function, but instead, the PT is via bubble like formation all across the matter. The bubble-like formation can make the PT take place instantly. However, such instances in the astrophysical scenario are difficult to observe in cold high-density matter.

## VI. SUMMARY AND CONCLUSION

In this present article, we mainly focus our attention on the effect of magnetic field on PT of an NS to QS. We have used relativistic MHS conservation condition to study this effect along with magnetic field induced EoS. For simplicity, we have chosen the HT frame (where the magnetic and matter velocities are aligned in the rest frame of the front) and we have also assumed infinite conductivity. We aim to categorize the PT process, whether it is a fast burning detonation or a slow combustion deflagration. In our calculation, we have used hadronic and quark EoS which is consistent with recent constraints. We have assumed magnetic fields of strength  $10^{15}$  G at the surface of the star which is usually observed in magnetars. The central magnetic field is considered to be of the order of  $1.7 \times 10^{18}$  G. Such magnetic fields are typically present at the cores of NS where the density is usually higher than 3 times saturation density  $\rho_s$ . In our calculation, we were studying the various quantities as a function of baryon density  $\rho_b$ . The baryon density which is relevant in our study is usually higher than 3 times  $\rho_s$ .

The energy of NM is higher than that of QM at higher densities, and the process can be exothermic. Therefore, the PT induced by shock like discontinuity at the star center would propagate outwards, converting NM to QM. We have also studied the quark to hadronic density ratio at the phase boundary and found that for the higher incoming velocity of NM the NM at the star core is unstable as compared to QM where the densities are greater than  $3\rho_s$ , and the NS would eventually convert to a QS. Similar, observation also came from comparing the pressure difference between the two phases.

Observing the criterion for the detonation and deflagration, we found that the velocity of the NM in most of the density range is greater than that of the speed of QM, which is the condition for a deflagration. Also, the  $(e - p)$  comparison of the respective phases comes to the same conclusion. The burning process at the star center most likely starts as a deflagration process. However, in almost all the curves we have found that there is a

small density window at lower densities where the process can be a detonation one. In this little window, all the parameters behave differently than for the deflagration case. However, from the energy plots, we find that at such low densities the NM energy and QM energy are almost equal. Therefore, at such densities, it is not likely that the PT process would be an exothermic one. The criterion for detonation and deflagration depends strongly on the choice of EoS and for further study different EoS sets could be employed.

Most of the exciting and new physical insight comes when we compared the magnetic field of the unburned NM and burned QM. At small enough infalling matter velocities the resultant magnetic field of the QS is lower than that of the NS. However, for the higher value of infalling matter velocities the magnetic field of QM becomes larger. Therefore, depending on the initial density fluctuation and on whether the PT is a violent one or not the QS could be more magnetic or less magnetic. This can have substantial observational significance because a strong magnetar can suddenly become less magnetic and would not show common magnetar properties like anomalous x-ray pulses and flares. On the other hand, a normal NS could suddenly start to exhibit x-ray pulses and giant flashes and other magnetars characteristics. And this change can happen suddenly as the PT is a fast process.

The sudden PT can also have a massive effect on the magnetic tilt of the star. For smaller velocities and densities the magnetic inclination are not affected much but for higher infalling velocities tilt of the magnetic axis can change suddenly with PT. In such extreme cases, the magnetic angle suddenly changes sign and even can increase quite a lot suddenly. All previous calculation regarding the evolution of magnetic tilt axis is a slow process and is connected with its lifetime and speed. However, the change in the magnetic tilt for magnetars due to PT is a sudden process and is also an interesting one. Which can mean that a star with MA tilted to the right can undergo a PT and the resultant QS can have an MA tilted to the left. This can have a considerable effect on the observation of the pulsars. A pulsar which was previously recorded can undergo a PT and can completely disappear from us. On the other hand, we can suddenly identify a new pulsar in the sky after it has undergone PT without any supernovae happening in the near past.

The TL shock was found difficult to initiate in this astrophysical scenario in the PT of NSs. However, it may be because we were only examining the case of step like discontinuity at the star center and had neglected bubble like PT scenario.

Although we have in detail discussed the magneto-hydrostatic scenario of the PT of NS to

QS, we have here only established the initial conditions and the possible PT mechanism. The actual dynamic of the PT would be complete once we study and understand the magneto-hydrodynamic PT scenario solving the dynamic Euler's equations. Although such calculation would be very involved, it is on our immediate agenda.

## ACKNOWLEDGMENTS

RM would like to thank SERB, Govt. of India for monetary support in the form of Ramanujan Fellowship and Early Career Research Award. RM and AS would like to thank IISER Bhopal for providing all the research and infrastructure facilities.

- 
- [1] Weber, F., Pulsar as an astrophysical laboratory for nuclear and particle physics, (Institute of Physics Publishing, Bristol, 1999)
  - [2] Glendenning, N. K., Compact Stars: Nuclear Physics, Particle Physics, and General Relativity, (Springer, New York, 2000)
  - [3] Hewish A., Bell S. J., Pilkington J. D. H., Scott P. F. & Collins R. A., Nature 217, 709 (1968)
  - [4] Gold T., Nature 218, 731 (1968)
  - [5] Demorest, P., Pennucci, T., Ransom, S., Roberts, M., & Hessels, J., Nature, 467, 1081 (2010)
  - [6] Antonidis, J., Freire, P. C. C., Wex, N. et. al., Science, 340, 448 (2013)
  - [7] N. Itoh, Prog. Theor. Phys. 44, 291 (1970)
  - [8] A. R. Bodmer, Phys. Rev. D 4, 1601 (1971)
  - [9] Witten, E., PRD 30, 272 (1984)
  - [10] N. K. Glendenning, Nucl. Phys. B Proc. Suppl. 24, 110 (1991), Phys. Rev. D 46, 1274 (1992)
  - [11] C. Alcock, E. Farhi & A. Olinto, AstroPhys. J. 310, 261 (1986)
  - [12] A. Drago, A. Lavagno & G. Pagliara, Eur. Phys. J. A 19, 197 (2004)
  - [13] I. Bombaci & B. Datta, AstroPhys. J. 530, L69 (2000)
  - [14] Z. Berezhiani, I. Bombaci, A. Drago, F. Frontera & A. Lavagno, AstroPhys. J. 586, 1250 (2003)
  - [15] R. Mallick & P. K. Sahu, Nucl. Phys. A 921, 96 (2014)
  - [16] A. Sedrakian, Astron. & Astrophys. 555, L10 (2013)

- [17] E. B. Abdikamalov, H. Dimmelmeier, L. Rezzolla & J. C. Miller, *Mon. Not. R. Astron. Soc.* 392, 52 (2009)
- [18] J. E. Horvath, *Int. J. Mod. Phys. D* 19, 523 (2010)
- [19] A. Drago, A. Lavagno & I. Parenti, *Astrophys. J.* 659, 1519 (2007)
- [20] A. Bhattacharyya, S. K. Ghosh, P. S. Joarder, R. Mallick & S. Raha, *Phys. Rev. C* 74, 065804 (2006)
- [21] L. M. Lin, K. S. Cheng, M. C. Chu & W. -M. Suen, *Astrophys. J.* 639, 382 (2006)
- [22] Olinto, A., *Phys. Lett. B*, 192, 71 (1987)
- [23] Horvath, J. E., & Benvenuto, O. G., *Phys. Lett. B*, 213, 516 (1988)
- [24] Cho, H. T., Ng, K. W., & Speliotopoulos, A. D., *Phys. Lett. B*, 326, 111 (1994)
- [25] Mishustin, I., Mallick, R., Nandi, R. & Satarov, L., *Phys. Rev. C*, 91, 055806 (2015)
- [26] Kulkarni, S. R., and Frail, D. A., *Nature* 365, 33 (1993)
- [27] Murakami, T., Tanaka, Y., Kulkarni, S. R., et al., *Nature* 368, 127 (1994)
- [28] Duncan, R. C., and Thompson, C., *AstroPhys. J.* 392, L9 (1992)
- [29] Thompson, C., and Duncan, R. C., *AstroPhys. J.* 408, 194 (1993)
- [30] Paczynski, B., *Acta. Astron.* 42, 145 (1992)
- [31] Melatos. A., *Astrophys J. Lett.* 519, L77 (1999)
- [32] Makishima, K., Enoto, T., Hiraga, J. S. & et al., *Phys. Rev. Lett.* 112, 171102 (2014)
- [33] S. Akiyama, J. C. Wheeler, D. L. Meier, & I. Lichtenstadt, *Astrophys. J.* 584, 954 (2003)
- [34] M. Obergaulinger, P. Cerd-Durn, E. Mller, and M. Aloy, *Astron. Astrophys.* 498, 241 (2009)
- [35] H. Sawai and S. Yamada, *Astrophys. J.* 817, 153 (2016)
- [36] P. Msta, C. D. Ott, D. Radice, L. F. Roberts, E. Schnetter, & R. Haas, *Nature (London)* 528, 376 (2015)
- [37] T. Rembiasz, M. Obergaulinger, P. Cerd-Durn, E. Mller, & M. A. Aloy, *Mon. Not. Roy. Astron. Soc.* 456, 3782 (2016)
- [38] Mallick, R., Schramm, S., *Phys. Rev. C* 89, 025801 (2014)
- [39] Csernai, L. P., *Zh. Eksp. Teor. Fiz.* **92**, 379 (1987)
- [40] Serot, B. D., & Walecka, J. D., *Adv. Nucl. Phys.* 16, 1 (1986)
- [41] Boguta, J., & Bodmer, R. A., *Nucl. Phys. A* 292, 413 (1977)
- [42] Glendenning, N. K., & Moszkowski, S. A., *Phys. Rev. Lett.* 67, 2414 (1991)
- [43] J. Schaffner and I. N. Mishustin, *Phys. Rev. C* 53, 1416 (1996)

- [44] P. G. Reinhard, Z. Phys. A 329, 257 (1988).
- [45] Steiner, A. W., Lattimer, J. M., & Brown, E. F., Astrophys. J. 765, L5 (2013)
- [46] Lattimer, J. M., & Lin, Y., Astrophys. J. 771, 51 (2013)
- [47] A. Chodos, R. L. Jaffe, K. Johnson, C. B. Thorn & V. F. Weisskopf, Phys. Rev. D 9, 3471 (1974)
- [48] Mallick, R., & Sinha, M., MNRAS 414, 2702 (2011)
- [49] Mallick, R., and Schramm, S., Phys. Rev. C89, 045805 (2014)
- [50] Bandyopadhyay, D., Chakrabarty, S., Dey, P., & Pal, S., Phys. Rev. D, 58, 121301 (1998)
- [51] Dexheimer, V., Negreiros, R., & Schramm, S., Eur. Phys. J. A, 48, 189 (2012)
- [52] Furusawa, S, Sanada, T., & Yamada, S., Phys. Rev. D 93, 043018 (2016)
- [53] Furusawa, S, Sanada, T., & Yamada, S., Phys. Rev. D 93, 043019 (2016)
- [54] Taub, A. H., Phys. Rev. bf 74, 328 (1948)
- [55] de Hoffmann, F., & Teller, E., Phys. Rev. **80**, 692 (1950)
- [56] Flowers, E., & Ruderman, M. A., Astrophys. J., 215, 302, (1977)
- [57] Radhakrishnan, V., & Cooke, D. J., Astrophys. Lett., 3, 225 (1969)
- [58] Tauris, T. M., & Manchester, R. N., MNRAS, 298, 625 (1998)
- [59] Young, M. D. T., Chan, L. S., Burman, R. R., & Blair, D. G., MNRAS, 402, 1317 (2010)
- [60] Rookyard, S. C., Weltevrede, P., & Johnston, S., MNRAS, 446, 3367 (2015)
- [61] L. D. Landau & E. M. Lifshitz, Fluid Mechanics (Pergamon Press, 1987)